Reciprocating-flowing on-a-chip enables ultra-fast immunobinding for multiplexed rapid ELISA detection of SARS-CoV-2 antibody

Yiren Liu [a], Yayin Tan [a], Quanying Fu [a], Maoren Lin [b], Jinxu He [a], Suhua He [b], Mei Yang [b], Shoudeng Chen [b,**], Jianhua Zhou [a,*]

[a] Key Laboratory of Sensing Technology and Biomedical Instruments of Guangdong Province, School of Biomedical Engineering, Sun Yat-sen University, Guangzhou, 510275, China
[b] Guangdong Provincial Key Laboratory of Biomedical Imaging, The Fifth Affiliated Hospital, Sun Yat-sen University, Zhuhai, 519000, China

ARTICLE INFO

ABSTRACT

The worldwide epidemic of novel coronavirus disease (COVID-19) has led to a strong demand for highly efficient immunobinding to achieve rapid and accurate on-site detection of SARS-CoV-2 antibodies. However, hour-scale time-consumption is usually required to ensure the adequacy of immunobinding on expensive large instruments in hospitals, and the common false negative or positive results often occur in rapid on-site immunoassay (*e.g.* immunochromatography). We solved this dilemma by presenting a reciprocating-flowing immunobinding (RF-immunobinding) strategy. RF-immunobinding enabled the antibodies in fluid contacting with the corresponding immobilized antigens on substrate repeatedly during continuous reciprocating-flowing, to achieve adequate immunobinding within 60 s. This strategy was further developed into an immunoassay method for the sero-logical detection of 13 suspected COVID-19 patients. We obtained a 100% true negative and true positive rate and a limit of quantification (LOQ) of 4.14 pg/mL. Our strategy also can be a potential support for other areas related to immunorecognition, such as proteomics, immunopharmacology and immunohistochemistry.

1. Introduction

The outbreak of the coronavirus disease 2019 (COVID-19) has brought about the urgent call for the rapid and precise diagnosis of suspected COVID-19 patients using point of care testing (POCT) methods that are able to cover the demand for preliminary screening and on-site detection (Carter L. J. et al., 2020; Che et al., 2004; Diao et al., 2020; Sabino-Silva et al., 2020), especially the immunoassay methods for the serological detection of the antibodies against SARS-CoV-2 (Jiang et al., 2020; Liu et al., 2020; Shu et al., 2020). POCT requires a rapid, reliable, and portable detection method. Due to the requirement for expensive large instruments, some of the immunoassay techniques such as elec-trochemiluminescence are not preferred for preliminary screening, even if those methods are efficient and highly sensitive for the massive detection in hospitals (Gao et al., 2020). As a representation of POCT methods, paper-based lateral flow immunochromatography has been widely used for preliminary screening and on-site detection, because of its advantages of rapid, visualized detection and easy-to-use protocol.

However, immunochromatography also commonly accompanies by false positive or false negative results, which deteriorated the evalua-tions about its reliability and repeatability (Bowen Raffick A. R. et al., 2005; Narita et al., 2019). Conventional enzyme-linked immunosorbent assay (ELISA) that is typically functioned on a micro-plate (*e.g.* 96-well plate) is another option for preliminary screening due to its advantages of low cost and high sensitivity. These plate-based ELISA are convenient because each step of the detection procedure in these methods can be achieved manually without any assistance of extra instruments. (Lee et al., 2009; Li et al., 2014; Parween and Nahar 2013). But conventional ELISA usually consumes hour-scale time for immunobinding, and this labor-intensive, time-consuming protocol restrains its potential in POCT for on-site detection (Herrmann et al., 2008; Lai et al., 2004; Lee et al., 2009; Sato et al., 2004).

In the recent decade, researchers have developed microfluidic ELISA by pre-loading all reagents into a chip, and then transferring the re-agents into reaction chambers in order when testing. The microfluidic ELISA integrates most steps of conventional ELISA into an on-chip

detection protocol so that the time consumption of detection is reduced to almost 30 min (Christodoulides et al., 2002; Endoa et al., 2005; Herrmann et al. 2006, 2008; Hiroyuki et al., 2005; Holmes et al., 2007; Lai et al., 2004; Lee et al., 2009; Liu et al., 2005; Murakami et al., 2004; Peoples and Karnes 2008; Riegger et al. 2006, 2007; Sandro et al., 2004; Sato et al., 2004; Tamarit-López et al., 2008). With the addition of extra devices and control systems, the control such as centrifugal control or magnetic control of these microfluidic ELISA might re-increase the cost of ELISA (Endoa et al., 2005; Herrmann et al. 2006, 2008; Hiroyuki et al., 2005; Holmes et al., 2007; Murakami et al., 2004; Sato et al., 2004; Tamarit-López et al., 2008). Some ELISA chips still adopt static immunobinding in certain chambers to obtain adequate immunobinding by prolonging time-consumption (Christodoulides et al., 2002; Lai et al., 2004; Lee et al., 2009; Liu et al., 2005; Riegger et al. 2006, 2007; Sandro et al., 2004). Several ELISA chips speed up the immunobinding by introducing the flow-through flowing manners on the chip. In these flow-through immunobinding methods, the fluid actually flows in one direction. Take indirect ELISA as example, the antibodies in the fluid usually have only one chance to contact with the pre-coated antigens on the substrate, which reduced the time-consumption indeed but weakened the adequacy of immunobinding (Endoa et al., 2005; Herrmann et al. 2006, 2008; Hiroyuki et al., 2005; Holmes et al., 2007; Murakami et al., 2004; Sato et al., 2004; Tamarit-López et al., 2008). These current formats of immunobinding have restrained the POCT potential of ELISA. More than that, since immunobinding is the crux of most immunoassay techniques, such as electrochemiluminescence immunoassay and immunochromatography, the performances of most other immunoassay techniques might be also restrained due to the insufficient immunobinding at small volume of sample and short detection time (Liu et al., 2020).

In our previous works, we had found the improvements of on-chip cell culture due to the flow renewal (Zhou et al., 2011). Herein, we presented a novel strategy for an immunobinding method under a flow renewal, the reciprocating-flowing immunobinding (RF-immunobinding) on a chip. In this RF-immunobinding strategy, the sample fluid was reciprocated in the chip microchannel under the pressure regulation. We demonstrated the fluid behaviors during the controllable reciprocating-flowing by video-recording and angiography. By introducing the reciprocating-flowing, the sample fluid was reciprocated through the detection site for multiple times, to enable the repeatable contact between the antibodies carried in fluid and the corresponding antigens pre-coated at the substrate. With the effect of this enhanced collision, the time-consumption for adequate immunobinding could be reduced to less than 1 min as shown by the results of binding dynamics, which was approximate to 10.8% of that required for static immunobinding.

The on-chip RF-immunobinding strategy was further developed into a reciprocating-flowing ELISA chip (RF-ELISA chip) and applied to the serological detection of the antibodies that were specific to the nucleoprotein antigens of SARS-CoV-2 from the serum of 13 suspected COVID-19 patients. The detection using RF-ELISA chip could be completed within 5 min in which each step of immunobinding required 1–2 min only, and achieved a 100% true negative and positive rate for qualitative detection and a limit of quantification (LOQ) of 4.14 pg/mL for quantitative detection, which indicated that the RF-ELISA holds reliable potential for rapid trace immunoanalysis.

2. Materials and methods

2.1. Chip fabrication

The chip could be fabricated without a professional laboratory. All the necessary requirements are the following: the heating equipment such as an experiment-used drying oven or home-used oven that could cure the PDMS or other material, the adhesive agent such as normal glue that could bond the flat glass with the layer with microchannels, and the

vessel such as Petri dish or household aluminum (Al) foil paper for containing the mold. The reagents and the fabrication details were shown in the Supplementary Materials (Experimental section and Fig. S1).

2.2. Methodology: two-step RF-ELISA (one-step immunobinding)

The procedure of serological detection using two-step RF-ELISA was shown in Fig. S2. Firstly, we prepared the HRP conjugated second antibody solution (mixing with PBS in dilution 1:250), then mixed it with the model antibody (*i.e.* anti-(human)-SARS-CoV-2 nucleoprotein taken from rabbit) or serum sample in dilution 1:1 to prepare sample solution. After loading the sample solution into the inlet chamber, we controlled the pressure regulation to enable the sample solution flowing forward and backward by slightly squeezing and releasing the pure water bottle for 1–2 min at 37 °C. After that, we discharged the sample solution from the buffer chamber, and washed out the residual reagents in microchannels with phosphate buffered saline-tween-20 (PBST, pH 8.0). Afterward, we loaded the mixture of 3,3',5,5'-tetramethylbenzidine (TMB) and H_2O_2 into the inlet chamber, repeated the pressure regulation for 1–2 min in 37 °C to start the catalytic reaction, then we added 2.0 M H_2SO_4 to end the catalytic reaction.

Each step of immunobinding and the catalytic reaction were all finished within 2 min, and the whole detection procedure required less than 5 min. The detection was carried out by using a visual colorimetry and the following imaging analysis. The simple device for detection was composed of a RF-ELISA chip, a smart phone and a software for imaging analysis, and the details of the device were shown in Fig. S3.

2.3. Statistical analysis

We performed the statistical comparison of colorimetric results on each chip detection by One-Sample t-Test to evaluate whether the significant difference between the blank/control sample and the unknown samples exists. The average gray level of PBS blank or serum 1 was used as the test mean to statistically compare with the colorimetric results of other samples taken from the same chip detection. And the data were expressed as the mean ± standard deviation (SD). Those statistical analysis was performed using software ORIGIN PRO (OriginLab, Inc., Massachusetts, USA). We considered the significant difference existing with a value of $P < 0.05$. Particularly, we marked the significant difference with P value > 0.05 as Not Significant (N.S.), $0.01 < P$ value < 0.05 as *, $0.001 < P$ value < 0.01 as **, P value < 0.001 as ***, respectively.

3. Results and discussion

3.1. The principle of RF-immunobinding

The structure of the chip was shown in Fig. 1A and the principle of the RF-immunobinding was displayed in Fig. 1B. The RF-ELISA chip was assembled with an antigen-coated glass substrate, a microchannel layer fabricated with PDMS or slime, and a pressure regulating modular such as a pure water bottle, as illustrated in Fig. 1A. The fabrication of this chip was characterized by its simplicity and cheapness.

The state of reciprocating-flowing in the channel of a RF-ELISA chip was demonstrated in Fig. 1B. After loading the sample into the inlet chamber, the fluid that carried with the antibodies would flow into the microchannel and pass through the detection site that was pre-coated with the corresponding antigens. The natural flowing of the fluid was shown in Fig. 1B i). The coated antigens at the detection site would contact and react with the corresponding antibodies carried in the sample fluid. Theoretically, by introducing a pressure regulation that was shown in Fig. 1B ii), and Fig. 1B iii), the natural flowing was thus regulated into a controllable reciprocating-flowing that enabled the sample fluid flowing through the detection site repeatedly. In the
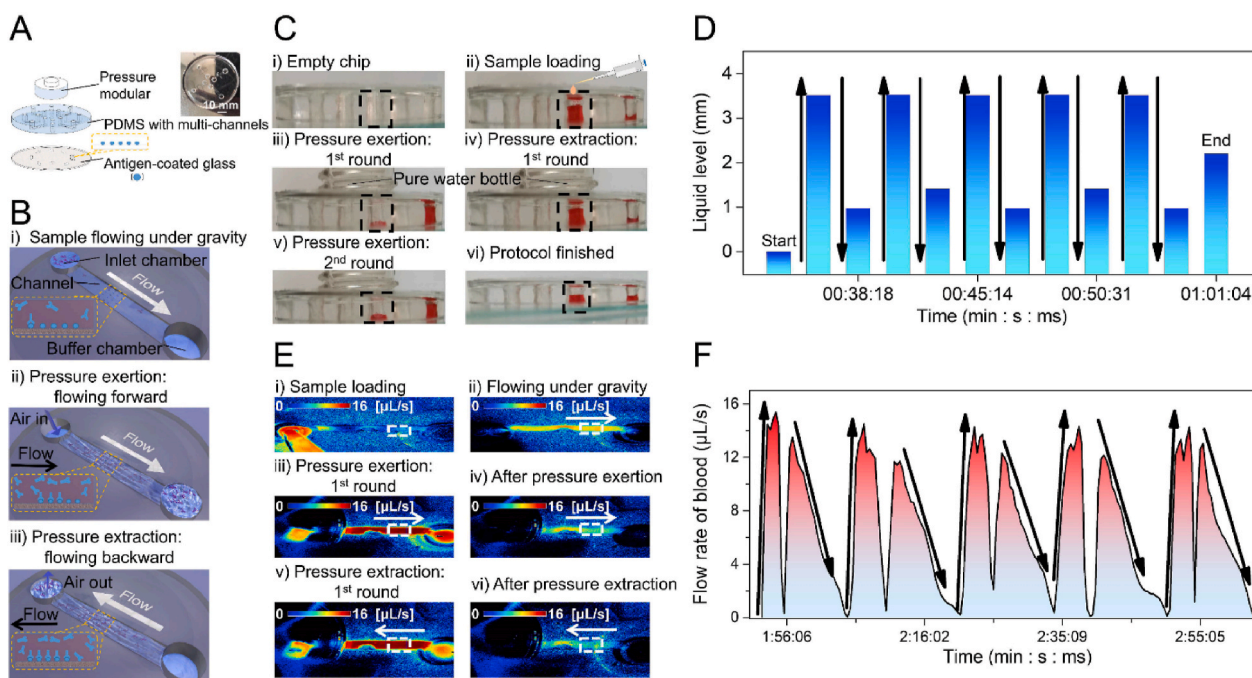
Fig. 1. The principle of RF-immunobinding. (**A**) The structure of the chip, inset: the top-view photograph of the chip. (**B**) The schematics of the state of sample flow in different step of RF-immunobinding. (**C**) The time-dependent fluid level in the inlet chamber. (**D**) The time-dependent changes of the fluid level in inlet chamber for five rounds. (**E**) The flow rate distribution of blood in microchannel. (**F**) The time-dependent flow rate of the blood at the detection site for five rounds.

process of reciprocating-flowing, the fluid carrying with antibodies is able to repeatedly collide with the antigens pre-coated on the glass substrate, to realize the multiple contact of the antibodies and antigens. This enhanced collision and improved contact probability would reduce the time-consumption on the premise of the adequate immunobinding. To further investigate the flow behaviors of reciprocating-flowing in the microchannel under pressure regulation, we simulated the changes of flow direction and flow rate during the process of reciprocating-flowing by ANSYS software on the computer. The details of the simulation were shown in the Supplementary Materials (Experimental section, Fig. S4 and Movie S1&S2). The results of simulation were consistent with our proposal.

Supplementary video related to this article can be found at htt ps://doi.org/10.1016/j.bios.2020.112920

To confirm the changes of flow direction and flow rate in the process of reciprocating-flowing that was regulated by a pure water bottle as a control modular, we measured and visualized the real fluid behaviors during reciprocating-flowing, as shown in Fig. 1C–F. To indicate the flow direction changes, we observed the fluid level of red ink (as the mimic of blood) inside the inlet chamber under pressure regulation (Fig. 1C and Movie S3). After loading the red ink into the inlet chamber of an empty chip (Fig. 1C i)), the ink would flow to the buffer chamber under gravity, but most ink stayed in the inlet chamber due to the hydrophobicity of the PDMS channel (Fig. 1C ii)). After that, we sealed the inlet chamber with a pure water bottle (bottleneck facing down), then regulated the pressure in the chambers and microchannel by pressing and releasing the bottle. Firstly, we squeezed the bottle slightly then held still to generate the compressed air at a certain volume to function the 1st round of pressure exertion until most ink flowing into the buffer chamber. The compressed air forced most ink flowing through the microchannel and to the buffer chamber, leading to the rapid decrease of the fluid level in the inlet chamber (Fig. 1C iii)). Afterward, to function the 1st round of pressure extraction, we slowly released the bottle to drive the ink flowing backward into the inlet chamber, which re-rose the fluid level in inlet chamber (Fig. 1C iv)). We repeated the processes of pressure exertion and pressure extraction to maintain the continuous reciprocating-flowing (Fig. 1C v)) until the protocol finished (Fig. 1C

vi)). We measured the fluid level on each step of the five rounds of pressure regulation, which suggested that a pure water bottle could control the fluid flow direction during reciprocating-flowing in the microchannel as required, as shown in Fig. 1D.

To indicate the changes of flow rate under pressure regulation, we also visualized the flow behaviors by imaging the reciprocating-flowing of blood solution with the assistance of a pure water bottle on a BVI system, as shown in Fig. 1E and Movie S4. Firstly, we loaded the diluted human blood (mixing with PBS buffer in dilution 1:1) into the inlet chamber (Fig. 1E i)). In the beginning, the blood solution flowed through the detection site slowly under gravity (Fig. 1E ii)). Then we applied the pressure regulation following the same process in the fluid level observation in Fig. 1C. As shown in Fig. 1E iii), the pressure exertion process significantly improved the flow rate of the fluid, to enable the blood solution flowing forward and through the detection site with a high flow rate. After that, the flow rate gradually slowed down due to the loss of the pressure from compressed air (Fig. 1E iv)). In and after the process of pressure extraction, the blood solution flowed backward through the detection site (Fig. 1E v) and vi)), and the changes of the flow rate were corresponding to the situation of pressure exertion. We recorded the time-dependent changes of flow rate under continuous reciprocating-flowing, as shown in Fig. 1F. The flow rate was changed uniformly at each position of the flowing fluid, and the rate of these flow rates changing with time broadly remained stable during each period of pressure regulation. The results revealed that the format of the reciprocating-flowing was laminar, in accordance with the state of our simulation emulated.

The measurements and visualization above testified that a simple tool such as a pure water bottle is sufficient to meet requirement of pressure regulation to generate controllable, continuous reciprocating-flowing in chambers and microchannels. These flow behaviors are consistent with the simulation of the reciprocating-flowing in the microchannel of the RF-ELISA chip, as shown in Fig. S4 and Movie S1&S2, supporting the feasibility of our proposed strategy.

Supplementary video related to this article can be found at htt ps://doi.org/10.1016/j.bios.2020.112920

3.2. *The dynamics of antibodies binding onto the corresponding antigens immobilized on the substrate*

To monitor the binding process of antibodies and antigens during reciprocating-flowing, we measured the dynamics of anti-SARS-CoV-2 nucleoprotein binding onto the corresponding immobilized antigens on a spectral-domain phase sensitive interferometry (SD-PSI) in real-time (Fig. 2). In the measurements by using SD-PSI, the time-dependent changes of relative thickness (RT) of the immobilized matters on the detection substrate would be detected sensitively. In our dynamics experiments, the more the RT increased, the more anti-SARS-CoV-2-nucleoprotein antibodies had been captured and bound to the immobilized nucleoprotein antigens on the glass substrate.

In the dynamics experiments of RF-immunobinding, with the assistance of pressure regulation, the sample fluid flowed through the detection site for multiple times in the microchannel, which enabled the repeatable contact between the antibodies carried in the sample fluid

and the antigens coated at the detection site (Fig. 2A a)). As shown in Fig. 2B a), after the sample loading and pressure regulating were completed at about the 176th s, the dynamics curve of 434.0 ng/ml antibody (mixing with PBS) binding onto coated antigen reached equilibrium at about the 233rd s. After that, the immobilized antigens at the detection site captured no more anti-SARS-CoV-2 nucleoprotein, which indicated that the adequate immunobinding of 434.0 ng/ml antibody and the corresponding immobilized antigen could be completed in about 57 s (<1 min) under reciprocating-flowing.

For static immunobinding, the binding between antibodies carried in fluid and corresponding immobilized antigens was mainly controlled by the free diffusion of antibodies (Fig. 2A b)). As shown in Fig. 2B b), after the sample loading was completed at about the 160th s, the dynamics curve reached equilibrium at about the 660th s, indicating that the immunobinding of 434.0 ng/ml antibodies with the immobilized antigens was completed in about 527 s in a static system. The time-consumption of static immunobinding was approximate to 9.25 folds
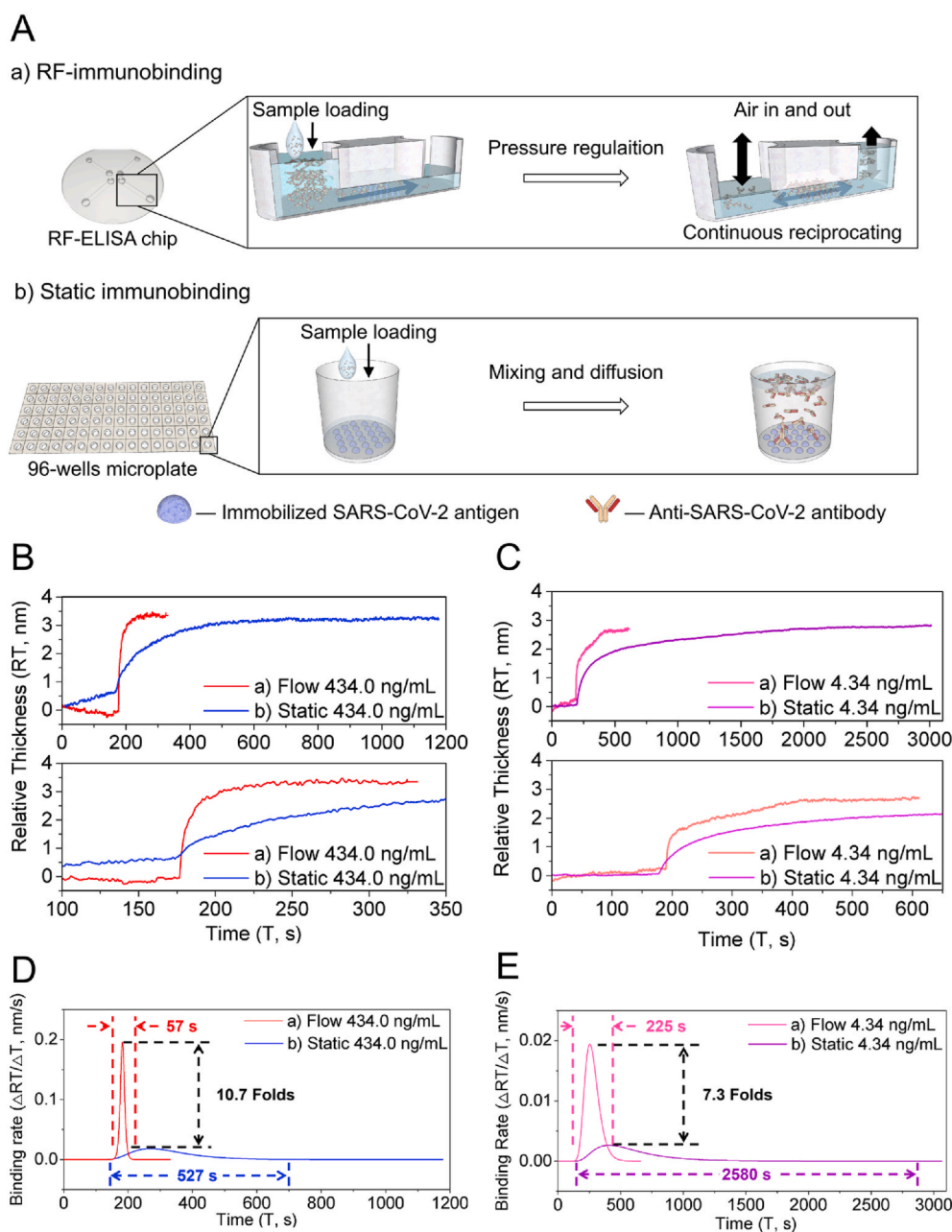

Fig. 2. The dynamics of anti-SARS-CoV-2 antibody binding onto immobilized SARS-CoV-2-nucleoprotein antigen, measuring by SD-PSI in real-time. (**A**) The schematic diagram showing the binding between antibody and antigen, **a**) in continuous reciprocating-flowing and **b**) in static system. (**B**) Sensorgram obtained from the binding of anti-SARS-CoV-2 nucleoprotein (434.0 ng/mL) to nucleoprotein antigen of SARS-CoV-2 in **a**) reciprocating-flowing and **b**) static system, upper: measuring in real-time from 0 s to 1200 s, below: measuring in real-time from 100 s to 350 s. (**C**) Sensorgram obtained from the binding of anti-SARS-CoV-2 nucleoprotein (4.34 ng/mL) to nucleoprotein antigen of SARS-CoV-2 in **a**) reciprocating-flowing and **b**) static system, upper: measuring in real-time from 0 s to 3100 s, below: measuring in real-time from 0 s to 650 s. (**D**) The first order derivative of the fitting curves taken from the dynamics curves for 434.0 ng/mL antibody solution. (**E**) The first order derivative of the fitting curves taken from the dynamics curves for 4.34 ng/mL antibody solution.

of that required for the RF-immunobinding.

We also repeated the dynamics experiments by binding 4.34 ng/ml antibody onto the coated antigen (Fig. 2C). The results showed that the binding of 4.34 ng/mL antibody to corresponding immobilized antigen required almost 43 min (about 2580 s) in static system, which was approximate to 11.5 folds of that required for RF-immunobinding (about 225 s).

In order to further elaborate the effect of reciprocating-flowing on immunobinding rate, we fitted those dynamics curves based on Boltzmann transport equation (BTE) (Fig. S5). Then, we differentiated these fitting curves respectively to obtain the curves of binding rate vs. time during the process of immunobinding. The curves of binding rate vs. time can be conductive to distinguish the disparities of time-consumption in RF-immunobinding and static immunobinding (Fig. 2D–E). In a first order derivative curve, the binding rate started raising from zero at the beginning of immunobinding. After that, the binding rate of antibody increased to its maximum, then reduced back to zero again, reaching the steady-state. At this state, the total amount of antibody binding to the substrate has been saturated. As the results in Fig. 2D–E shown, in the process that 434.0 ng/mL or 4.34 ng/mL antibodies bound to the immobilized antigens, the max binding rate of RF-immunobinding was 0.196 nm/s or 0.0194 nm/s, which was equal to 10.7 folds or 7.3 folds of that of static immunobinding (0.0182 nm/s or 0.00266 nm/s), respectively.

The results of binding dynamics above proved that the efficiency of RF-immunobinding was significantly higher than that of static immunobinding, indicating that the contact and reaction of immobilized antigens and its corresponding antibodies in fluid had been enhanced by the process of reciprocating-flowing. The strategy of RF-immunobinding can achieve such an ultra-fast, adequate immunobinding with reasonable stability and repeatability. These improvements required the simple control with a pure water bottle only. Our proposed RF-immunobinding thus had been authenticated.

3.3. The serological qualitative detection of anti-SARS-CoV-2 nucleoprotein using two-step RF-ELISA

Based on the study of RF-immunobinding that was regulated by pressure, we further developed a two-step RF-ELISA for the serological detection of anti-SARS-CoV-2 nucleoprotein, to confirm the reliability of RF-immunobinding in a real application. The serological detection of the suspected COVID-19 patients using the two-step RF-ELISA was shown in Fig. 3. Including sample loading, immunobinding and catalytic colorimetry, Fig. 3A described a schematic of the main steps in the detection procedure, and the experimental details were shown in Fig. S3 and Fig. S4. The qualitative detection of serum 1–3 was shown in Fig. 3B. The colorimetric result of phosphate-buffered saline (PBS) blank showed no significant difference with that of serum 1. Meanwhile, the colorimetric result of PBS blank was significantly different from those of serum 2 and 3. To double-check the result correctness of serum 1, we put it into the next detection and detected it again with serum 4 and 5 (Fig. 3C). Due to the consistent reports of the negative responses of serum 1 in the two detections, we considered serum 1 as a negative sample and set it as a negative control in the following qualitative detection of serum 6–13 (Fig. 3D–F). The colorimetric results of the qualitative detection for the 13 serum samples showed none of false positive or false negative results using two-step RF-ELISA, compared with clinical results from the fifth affiliated hospital of Sun Yat-Sen University (FAH-SYSU), as shown in Fig. 3G and Table S1.

Based on the concentration-dependent responses of colorimetric results in gray level, we obtained the results for semi-quantitative detection of the samples on the same chip. We displayed the semi-quantitative results taken from our two-step RF-ELISA and conventional static ELISA performed in FAH-SYSU, respectively (Fig. S7). The threshold in the two-step RF-ELISA detection was defined as the sum of average value of blank and two times of standard deviation (SD). According to the

comparison in Fig. S7, RF-ELISA detection could identify the basic status of each patient as correctly as the clinical detection, such as the negative or positive results of suspected COVID-19 infection.

3.4. The serological quantitative detection of anti-SARS-CoV-2 nucleoprotein using two-step RF-ELISA

Moreover, we repeated the detection for serum 6–10 by using a six-channel RF-ELISA chip (Fig. S6). The qualitative or semi-quantitative results were consistent with those taken from the detections using four-channel chips. It suggested that we can design and fabricate different patterns of the microchannels on the chips for multipurpose of immunoanalysis. In order to evaluate the performances of the two-step RF-ELISA for rapid quantitative detection, firstly, we performed the quantitative detection of a model antibody with six concentrations on a six-channel RF-ELISA chip, and established the linear regression equation of presented RF-ELISA (Fig. 4A and Fig. S8A). According to the quantitative results for the model samples, the correlation coefficient of the standard curve was $R^2 = 0.997$ with mean CV < 10%, and the LOQ in this detection was 4.14 pg/mL. Then we repeated the quantitative detection of model antibodies by using the conventional static ELISA adopted by FAH-SYSU, to establish the linear regression equation of a standard reference, as shown in Fig. 4B and Fig. S8B. We quantified all the serum samples based on the standard curves of two-step RF-ELISA and conventional static ELISA adopted by FAH-SYSU, respectively. The quantitative results of each serum sample were displayed in a correlation curve, which showed a linear correlation between the results taken from RF-ELISA and the conventional static ELISA (Fig. 4C). Compared with conventional ELISA (Fig. S9), the detection procedure was significantly speeded up in RF-ELISA on the premises of reliable reports, which means the RF-immunobinding is able to give consideration to both high efficiency and adequacy of immunobinding.

At last, we repeated all the serological detection experiments by developing a three-step RF-ELISA. In the three-step RF-ELISA, we introduced the serum sample solution into the detection sites first to make the target antibodies to be captured. After washing with PBST, we introduced the HRP-conjugated second antibody solution for another immunobinding. Three-step RF-ELISA is theoretically able to ensure the more accurate immunorecognition, but the time-consumption is almost double of that required for two-step RF-ELISA. The results of qualitative detection and the performances of quantitative detection were similar to those obtained from the two-step RF-ELISA, as shown in Fig. S10. Without any false negative or false positive results in the qualitative detection above, we proved that RF-ELISA allowed for the precise reports of true negative or positive results in real serological detection.

Furthermore, compared with conventional static ELISA methods, immunochromatography methods and electrochemiluminescence methods, RF-ELISA combined all the advantages of these three methods in the following four aspects: sample consumption, detection speed, LOQ and POCT potential (Table 1) (Boonham et al., 2014; Leng et al., 2008; Liu et al., 2015; Miao 2008; Ngom et al., 2010; Posthuma-Trumpie et al., 2009).

4. Conclusion

In conclusion, we proposed a strategy of controllable lab-on-a-chip RF-immunobinding with the assistance of pressure regulation. Combined with ELISA, the RF-immunobinding was further developed into the RF-ELISA for the serological detection of anti-SARS-CoV-2 nucleoprotein, with a time-consumption of less than 5 min for each detection. The detection results of 13 suspected COVID-19 patients indicated that RF-ELISA chip allowed for precise diagnosis with a 100% true positive and negative rate, a linear correlation coefficient of $R^2 = 0.997$, the mean CV less than 10% and the LOQ of 4.14 pg/mL. It is worth mentioning that, this chip was manually fabricated with simple tools, and the pressure regulation can be controlled easily by using a pure
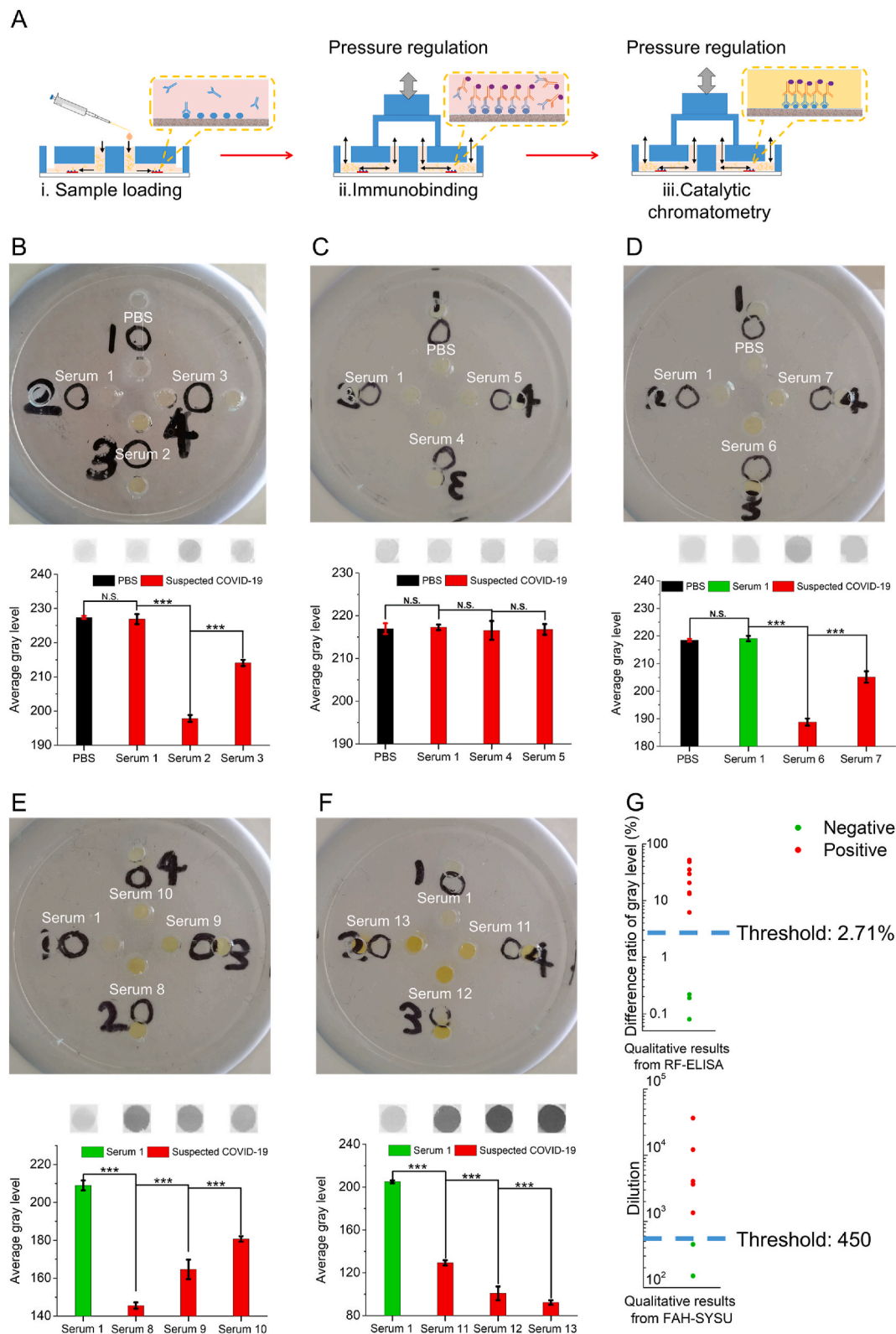
Fig. 3. The qualitative serological detection of the anti-SARS-CoV-2 nucleoprotein using the two-step RF-ELISA. (**A**) The schematics of the main steps for the detection. The qualitative detection of (**B**) PBS blank and serum 1–3; (**C**) PBS blank, serum 1 and serum 4–5; (**D**) serum 1 and serum 6–7; (**E**) serum 1 and serum 8–10; (**F**) serum 1 and serum 11–13. Upper: the images of the chips displaying colorimetric results, below: the images of the selected sites and its concentration-dependent responses in gray level. (**G**) The comparison of qualitative results taken from our presented RF-ELISA (upper) and conventional static ELISA performed in FAH-SYSU (below), respectively.
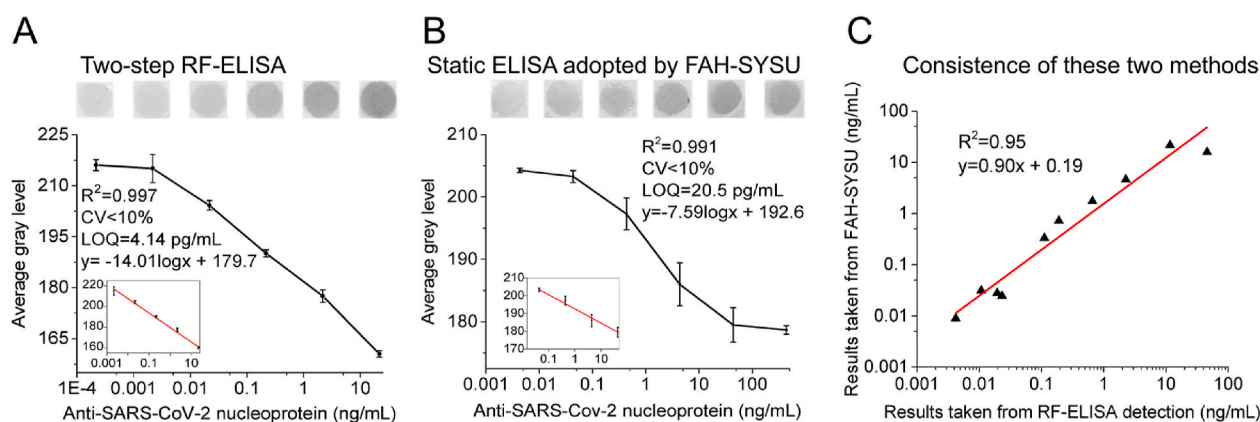
Fig. 4. The performances of quantitative detection by using two-step RF-ELISA. The quantitative detection of the model antibody by using (**A**) our two-step RF-ELISA; (**B**) conventional static ELISA adopted by FAH-SYSU. Upper: the images of the selected sites, below: corresponding concentration-dependent gray level. Insets: the linear regions of these two methods. (**C**) The linear correlation between the results of the serological detections taken from two-step RF-ELISA and conventional static ELISA adopted by FAH-SYSU, respectively.

Table 1

The comparison of the performances among conventional static ELISA, immunochromatography, electrochemiluminescence, and our RF-ELISA.

Methods	Performances					
	Volume consumption of sample	Time consumption of detection	Flow manner	LOQ (g/mL)	Cost	POCT potential
Our RF-ELISA	30–50 μL	4–5 min	Reciprocating-flowing	~4 E-12	Low	High
Conventional static ELISA	100–300 μL	>40 min	Static	~1.0 E-9	Low	Low
Immuno-chromatography	30–70 μL	10–15 min	Flow-through	~1.0 E-9	Low	High
Electro- chemiluminescence	100–300 μL	<20 min	Static or flow-through	>1.0 E-15	High	Low

water bottle. However, the manual fabrication of RF-ELISA chip might bring about the inconsistence of channel sizes, and the simple tools for pressure regulation might lead to the fluctuation of flow rate. We believe those disadvantages could be overcome by the introduction of auto-mated instruments for chip fabrication and pressure control. In the foreseeable future, with the assistance of automated instruments, we consider the RF-immunobinding will be not only a strong support for the preliminary diagnosis and on-site detection of community and primary clinics, but will also display a bright blueprint for providing better ef-ficiency and adequacy for significant works on many areas relevant to immunologic recognition, such as immunoassay, proteomics, immuno-pharmacology and immunohistochemistry.

Ethical approval

This study protocol was reviewed and approved by the Research Ethics Committee of the Fifth Affiliated Hospital of Sun Yat-sen University (No. ZDWY[2020] Lunzi No. (K22-1). Written informed consents were obtained from all patients.

Data and materials availability

All data needed to evaluate the conclusions in the paper are pre-sented in the paper and/or the Supplementary Materials. Additional data related to this paper may be requested from the authors.

CRediT authorship contribution statement

Yiren Liu: Methodology, Data curation, Formal analysis, Writing - original draft, Chip design, Fluid simulation, Principle measurement and, Visualization, Binding dynamics, Serological immunoassay, Data processing, Statistical analysis, Writing. **Yayin Tan:** Data curation, Binding dynamics, Data processing. **Quanying Fu:** Chip design, manu-script revision. **Maoren Lin:** Serological samples extraction and purifi-cation, Serological immunoassay. **Jinxu He:** Data curation, Fluid simulation, Data processing. **Suhua He:** Serological samples extraction and purification. **Mei Yang:** Writing - original draft, Serological samples extraction and purification. **Shoudeng Chen:** Methodology, Serological immunoassay, Writing. **Jianhua Zhou:** Writing - original draft, Meth-odology, Serological immunoassay, Writing.

Appendix A. Supplementary data

Supplementary data to this article can be found online at https://doi. org/10.1016/j.bios.2020.112920.

References

Boonham, N., Kreuze, J., Winter, S., Van Der Vlugt, R., Bergervoet, J., Tomlinson, J., Mumford, R., 2014. Methods in virus diagnostics: from ELISA to next generation sequencing. Virus Res. 186, 20–31.

Bowen Raffick, A.R., George, D.T., Hortin, G.L., 2005. False-negative result for cocaine metabolites on a lateral-flow drug test slide corrected by dilution. Clin. Chem. 4 (4), 790–791.

Carter, L.J., Garner, L.V., Smoot, J.W., Li, Y.Z., Zhou, Q.Q., Saveson, C.J., Sasso, J.M., Gregg, A.C., Soares, D.J., Beskid, T.R., Jervey, S.R., Liu, C., 2020. Assay techniques and test development for COVID-19 diagnosis. ACS Cent. Sci. 6 (5), 591–605.

Che, X.Y., Hao, W., Wang, Y.D., Di, B., Yin, K., Xu, Y.C., Feng, C.S., Wan, Z.Y., Cheng, V. C.C., Yuen, K.Y., 2004. Nucleocapsid protein as early diagnostic marker for SARS. Emerg. Infect. Dis. 10 (11), 1947–1949.

Christodoulides, N., Tran, M., Floriano, P.N., Rodriguez, M., Goodey, A., Ali, M., Neikirk, D., McDevitt, J.T., 2002. A microchip-based multianalyte assay system for the assessment of cardiac risk. Anal. Chem. 74 (13), 3030–3036.

Diao, B., Wen, K., Chen, J., Liu, Y., Yuan, Z., Han, C., Chen, J., Pan, Y., Chen, L., Dan, Y., Wang, J., Chen, Y., Deng, G., Zhou, H., Wu, Y., 2020. Diagnosis of acute respiratory syndrome coronavirus 2 infection by detection of nucleocapsid protein. MedRxiv. https://doi.org/10.1101/2020.03.07.20032524.

Endoa, T., Okuyamab, A., Matsubaraa, Y., Nishib, K., Kobayashia, M., Yamamuraa, S., Moritaa, Y., Takamuraa, Y., Mizukamib, H., Tamiya, E., 2005. Fluorescence-based assay with enzyme amplification on a micro-flow immunosensor chip for monitoring coplanar polychlorinated biphenyls. Anal. Chim. Acta 531 (1), 7–13.

Gao, X.H., Zhu, Y., Huang, B., Tan, Y., Zhu, J., 2020. Don't throw the stethoscope away! Eur. Heart J. https://doi.org/10.1093/eurheartj/ehaa343.

Herrmann, M., Veres, T., Tabrizian, M., 2008. Quantification of low-picomolar concentrations of TNF-α in serum using the dual-network microfluidic ELISA platform. Anal. Chem. 80 (13), 5160–5167.

Herrmann, M., Veresb, T., Tabrizian, M., 2006. Enzymatically-generated fluorescent detection in micro-channels with internal magnetic mixing for the development of parallel microfluidic ELISA. Lab Chip 6 (6), 555–560.

Hiroyuki, T., Stephan, H., Per, A., Ulrika, L., Nobuo, H., 2005. Simultaneous multiple immunoassays in a compact disc–shaped microfluidic device based on centrifugal force. Clin. Chem. 51 (10), 1955–1961.

Holmes, D., Joseph, K.S., Roachb, P.L., Morgan, H., 2007. Bead-based immunoassays using a micro-chip flow cytometer. Lab Chip 7 (8), 1048–1056.

Jiang, H.W., Li, Y., Zhang, H.N., Wang, W., Yang, X., Qi, H., Li, H., Men, D., Zhou, J., Tao, S.C., 2020. SARS-CoV-2 proteome microarray for global profiling of COVID-19 specific IgG and IgM responses. Nat. Commun. https://doi.org/10.1038/s41467-020-17488-8.

Lai, S.Y., Wang, S.N., Luo, J.L., Lee, J., Yang, S.T., Madou, M.J., 2004. Design of a compact disk-like microfluidic platform for enzyme-linked immunosorbent assay. Anal. Chem. 76 (7), 1832–1837.

Lee, B.S., Lee, J.N., Park, J.M., Lee, J.G., Kim, S., Cho, Y.K., Ko, C., 2009. A fully automated immunoassay from whole blood on a disc. Lab Chip 9 (11), 1548–1555.

Leng, S.X., McElhaney, J.E., Walston, J.D., Xie, D.X., Fedarko, N.S., Kuchel, G.A., 2008. ELISA and multiplex technologies for cytokine measurement in inflammation and aging research. J. Gerontol. A-Biol. 63 (8), 879–884.

Li, Y.S., Liu, G., Fu, X., He, J., Wang, Z., Hou, J., Cao, X., Shi, W., Zhang, S., 2014. High-sensitive chemiluminescent ELISA method investigation for the determination of deoxynivalenol in rice. Food Anal. Method 3 (3), 656–660.

Liu, W., Liu, L., Kou, G., Zheng, Y., Ding, Y., Ni, W., Wang, Q., Tan, L., Wu, W., Tang, S., Xiong, Z., Zheng, S., 2020. Evaluation of nucleocapsid and spike protein-based enzyme-Linked immunosorbent assays for detecting antibodies against SARS-CoV-2. J. Clin. Microbiol. https://doi.org/10.1128/JCM.00461-20.

Liu, W.T., Zhu, L., Qin, Q.W., Zhang, Q., Feng, H., Ang, S., 2005. Microfluidic device as a new platform for immunofluorescent detection of viruses. Lab Chip 5 (11), 1327–1330.

Liu, Z., Qi, W., Xu, G., 2015. Recent advances in electrochemiluminescence. Chem. Soc. Rev. 44 (10), 3117–3142.

Miao, W.J., 2008. Electrogenerated chemiluminescence and its biorelated applications. Chem. Rev. 108 (7), 2506–2553.

Murakami, Y., Endo, T., Yamamura, S., Nagatani, N., Takamura, Y., Tamiya, E., 2004. On-chip micro-flow polystyrene bead-based immunoassay for quantitative detection of tacrolimus (FK506). Anal. Biochem. 334 (1), 111–116.

Narita, A., Suzuki, A., Nakajima, T., Takakubo, Y., Ito, J., Sasaki, A., Takagi, M., 2019. Assessing an alpha-defensin lateral flow device for diagnosing septic arthritis: reporting on a false-negative case and a false-positive case. Mod. Rheumatol. 4 (1), 156–160.

Ngom, B., Guo, Y., Wang, X., Bi, D., 2010. Development and application of lateral flow test strip technology for detection of infectious agents and chemical contaminants: a review. Anal. Bioanal. Chem. 397 (3), 1113–1135.

Parween, S., Nahar, P., 2013. Image-based ELISA on an activated polypropylene microtest plate–a spectrophotometer-free low cost assay technique. Biosens. Bioelectron. 48 (19), 287–292.

Peoples, M.C., Karnes, H.T., 2008. Microfluidic capillary system for immunoaffinity separations of c-reactive protein in human serum and cerebrospinal fluid. Anal. Chem. 80 (10), 3853–3858.

Posthuma-Trumpie, G.A., Korf, J., Van Amerongen, A., 2009. Lateral flow (immuno) assay: its strengths, weaknesses, opportunities and threats. A literature survey. Anal. Bioanal. Chem. 393 (2), 569–582.

Riegger, L., Grumann, M., Nann, T., Riegler, J., Ehlert, O., Bessler, W., Mittenbuehler, K., Urban, G., Pastewka, L., Brenner, T., Zengerle, R., Ducrée, J., 2006. Read-out concepts for multiplexed bead-based fluorescence immunoassays on centrifugal microfluidic platforms. Sensor. Actuat. A-Phys. 126 (2), 455–462.

Riegger, L., Grumann, M., Steigert, J., Lutz, S., Steinert, C.P., Mueller, C., Viertel, J., Prucker, O., Rühe, J., Zengerle, R., Ducrée, J., 2007. Single-step centrifugal hematocrit determination on a 10-\$ processing device. Biomed. Microdevices 9 (6), 795–799.

Sabino-Silva, R., Jardim, A.C.G., Siqueira, W.L., 2020. Coronavirus COVID-19 impacts to dentistry and potential salivary diagnosis. Clin. Oral Invest. 24 (4), 1619–1621.

Sandro, C.T., Dernick, G., Juncker, D., Buurman, G., Kropshofer, H., Michel, B., Fattinger, C., Delamarche, E., 2004. High-sensitivity miniaturized immunoassays for tumor necrosis factor α using microfluidic systems. Lab Chip 4 (6), 563–569.

Sato, K., Yamanaka, M., Hagino, T., Tokeshi, M., Kimura, H., Kitamori, T., 2004. Microchip-based enzyme-linked immunosorbent assay (microELISA) system with thermal lens detection. Lab Chip 4 (6), 570–575.

Shu, H., Wang, S., Ruan, S., Wang, Y., Zhang, J., Yuan, Y., Liu, H., Wu, Y., Li, R., Pan, S., Ouyang, Y., Yuan, S., Zhou, P., Shang, Y., 2020. Dynamic changes of antibodies to SARS-CoV-2 in COVID-19 patients at early stage of outbreak. Virol. Sin. https://doi.org/10.1007/s12250-020-00268-5.

Tamarit-López, J., Morais, S., Puchades, R., Maquieira, Á., 2008. Use of polystyrene spin-coated compact discs for micro immuno as saying. Anal. Chim. Acta 609 (1), 120–130.

Zhou, J.H., Ren, K., Dai, W., Zhao, Y., Ryan, D., Wu, H., 2011. Pumping-induced perturbation of flow in microfluidic channels and its implications for on-chip cell culture. Lab Chip 11 (13), 2288–2294.